

# Quantification of Margins and Uncertainties for Aerospace Systems using Stochastic Expansions

Thomas K. West IV\* and Serhat Hosder†

*Missouri University of Science and Technology, Rolla, MO, 65409*

Tyler Winter‡

*M4 Engineering Inc., Long Beach, CA, 90807*

The objective of this study was to demonstrate the use of stochastic expansions in the quantification of margins and uncertainties in complex aerospace systems. In this study, stochastic expansions, based on nonintrusive polynomial chaos, were utilized for efficient representation of uncertainty both in design metrics and associated performance limits of a system. Additionally, procedures were outlined for analyzing systems that contain different uncertainty types between the performance metrics and performance limits. These methodologies were demonstrated on three model problems, each possessing mixed (epistemic and aleatory uncertainty) which was propagated through the models using second-order probability. The first was a complex system of highly nonlinear analytical functions. The second was a multisystem, physics based model for spacecraft reentry. The performance metrics consisted of two systems used to determine the maximum g-load, the necessary bank angle correction, and maximum convective heat load along a reentry trajectory. The last model was a multidisciplinary model for the design and analysis of a High Speed Civil Transport. Overall, the methodologies and examples of this work have detailed an approach for measuring the reliability of complex aerospace systems as well as the importance of quantifying margins and uncertainties for the design of reliable systems.

## Nomenclature

$N_s$	Number of Samples	$U_{UP}$	Upper Performance Gate Uncertainty
$\alpha^*$	Generic Uncertain Function	$U_{LW}$	Lower Performance Gate Uncertainty
$\Psi$	Random Basis Function	$CR$	Confidence Ratio
$N_t$	Number of Terms in a Total-Order Polynomial Chaos Expansion	$\beta$	Confidence Level
$\alpha$	Deterministic Coefficient in the Polynomial Chaos Expansion	$\dot{q}$	Heat Flux ( $W/cm^2$ )
$n$	Number of Random Dimensions	$Pr$	Prandtl Number
$p$	Order of Polynomial Expansion	$\rho$	Density ( $kg/m^3$ )
$\xi$	Standard Input Random Variable	$\mu$	Dynamic Viscosity ( $kg/m\cdot s$ )
$F$	Performance Metric	$P$	Pressure (Pa)
$FL$	Lower Performance Limit	$h_0$	Total Enthalpy (J/kg)
$FU$	Upper Performance Limit	$h$	Enthalpy
$M_{UP}$	Upper Performance Gate Margin	$Le$	Lewis Number
$M_{LW}$	Lower Performance Gate Margin	$h_D$	Enthalpy of Diffusion (J/kg)
$U_F$	Performance Metric Uncertainty	$h_f^0$	Heat of Formation (J/kmol)
$U_{FU}$	Upper Performance Limit Uncertainty	$c_i$	Mass Fraction of Species i
$U_{FL}$	Lower Performance Limit Uncertainty	$\epsilon$	Wall Emissivity
		$\sigma$	Stefan-Boltzmann Constant ( $5.67 \times 10^{-8} W/m^2 - K^4$ )

\*Graduate Student, Department of Mechanical and Aerospace Engineering, Student Member AIAA.

†Associate Professor of Aerospace Engineering, Department of Mechanical and Aerospace Engineering, Senior Member AIAA.

‡Aerospace Engineer, 4020 Long Beach Blvd., Long Beach, CA, 90807, Member AIAA.

$T$	Temperature (K)	$\Psi$	Heading Angle (Deg.)
$U$	Velocity (m/s)	$s$	Down Range Distance (km)
$S$	Reference Area ( $m^2$ )		
$h$	Altitude (km)		
$m$	mass (kg)		
$r$	Orbital Radius (km)		
$\gamma$	Flight Path Angle (Deg.)		
$\theta$	Longitude (Deg.)		
$\phi$	Latitude (Deg.)		
$\sigma$	Bank Angle (Deg.)		
$\omega$	Planetary Body Rotation Rate (rad/s)		

<i>Subscripts</i>	
$w$	Wall Condition
$e$	Boundary Layer Edge Condition
$\infty$	Free Stream Condition
$r$	Radiation
$c$	Conduction
$d$	Diffusion

## I. Introduction

In complex engineering problems, reliability is a key component of the design process. Complex aerospace systems and models, including spacecraft and aircraft, may possess a significant amount of nondeterministic parameters and mission critical performance metrics that are subject to uncertainty. Quantifying this uncertainty in, not only designs, but also in performance limits is critical in understanding and quantifying the reliability of a system. Because of the importance of such systems and associated models, there is a strong need for simple, yet efficient and accurate approach to measure the confidence and reliability of complex aerospace systems.

Quantification of Margins and Uncertainties (QMU) is a methodology developed to facilitate analysis and communication of confidence for certification of complex systems. This is performed with quantified uncertainty and margin metrics obtained for various system responses and performance parameters.<sup>1</sup> In recent years, a number of studies were reported on the theoretical development and the application of the QMU concept. The description of the key elements of a QMU framework was presented by Sharp and Wood-Schultz,<sup>1</sup> who utilized the QMU methodology for the certification of nuclear weapons. Eardley et al.<sup>2</sup> described QMU as a formalism dealing with the reliability of complex technical systems, and the confidence which can be placed in estimates of reliability. They also investigated the main components (performance gates, margins, and uncertainties) of QMU methodology. Pilch et al.<sup>3</sup> presented the main ideas underlying QMU, who also emphasized the need to separate aleatory and epistemic uncertainty in QMU. Helton<sup>4</sup> presented a comprehensive study on the QMU, which included a detailed analysis of the concept with different representations of uncertainty. Romero<sup>5</sup> discussed the issues and needs in QMU of complex coupled systems. Pepin et al.<sup>6</sup> presented a practical QMU metric for the certification of complex systems, which allowed uncertainty both on the operating region and the performance requirement and was not restrictive to a probabilistic definition of the uncertainty. A QMU approach was used for the characterization of the operational limits of the supersonic combustion engine of a hypersonic air-breathing vehicle by Iaccarino et al.<sup>7</sup> A study by Lucas et al.<sup>8</sup> utilized the QMU methodology to study the reliability of a ring structure. Swiler et al.<sup>9</sup> studied various approaches to characterize epistemic uncertainty in the calculation of margins.

While significant work has been done in the area of QMU and its methodologies, it is important to further develop new methods for efficient, accurate, and comprehensive representation and quantification of margins and uncertainties for complex aerospace systems. The objectives of this work are twofold. The first objective is to demonstrate the use of stochastic response surfaces based on nonintrusive polynomial chaos (NIPC) to quantify the uncertainty in system performance metrics as well as performance boundaries. Previous work by Betti and Hosder<sup>10,11</sup> as well as Hosder, Walters, and Balch<sup>12,13</sup> in the area of using stochastic expansions based on NIPC as a means of efficient uncertainty quantification (UQ) has been extensively investigated. These works included studies involving the propagation of both aleatory (inherent) and epistemic (model-form) uncertainties through a variety of stochastic model problems. In general, polynomial chaos methods are based on a spectral representation of the uncertainty and can be significantly more efficient than traditional Monte Carlo simulations. An additional advantage of NIPC methods is that the deterministic model, such as a CFD code, is treated as a black-box as no intrusive changes to the model are needed to perform UQ analyses. The theory behind the polynomial chaos methodologies are both well-defined and well-understood<sup>14</sup> making it a solid and reliable method for UQ in complex aerospace simulations and as a key component in an accurate and efficient QMU framework.

The second objective of this work is to define procedures to calculate the margin and uncertainty metrics

for a QMU analysis of systems containing multiple types of uncertainty representation between the design and performance limits. In many engineering applications, it is possible and likely that the uncertainty in the design condition may be different than the representation of the performance boundaries. Representation may be a pure probabilistic representation, an interval based representation, or a combination of the two (i.e. mixed uncertainty.) It may also be possible that no uncertainty exists in performance limits. This may be typical when trying to meet some specific design criteria. The goal is to outline how measures can be made between these different uncertainty representations to provide an accurate estimation of the reliability of the system and/or performance metric.

Methodologies developed in this study are demonstrated on three stochastic model problems. The first is an analytical model consisting of highly nonlinear functions typically used in optimization testing. This is to demonstrate the capability of NIPC when applied to complex problems and the use of stochastic response surfaces to represent uncertainty as well as demonstrate their use in a QMU analysis. The analytical model or system has two performance metrics or outputs, each bounded by performance limits with a different uncertainty representation to demonstrate the above stated second objective of the current work. The second model problem is a multisystem, multiphysics spacecraft reentry model which consists of coupled reentry dynamics and heat load models to characterize design critical measurements of a spacecraft during reentry. These include the maximum g-load, the required bank angle correction, and the maximum heat load along the reentry trajectory. This model is intended to demonstrate the methodologies outlined in this work on a practical aerospace engineering application in the area of spacecraft systems. A third test problem is utilized to demonstrate the QMU of a system used for a multidisciplinary design and analysis of a high speed civil transport (HSCT). Key performance parameters that will be investigated include range and drag coefficient based on uncertainty in Mach number, angle of attack, wing sweep, and wing taper ratio.

The following section describes the methodology behind stochastic responses surfaces using polynomial chaos expansions and their use as a means of accurate and efficient uncertainty quantification. Section III briefly describes the different types of uncertainty (aleatory and epistemic) as well as a short description of the process for propagating mixed uncertainty through a model. Section IV describes the formulation of the QMU methodologies and how the stochastic response surfaces can be incorporated into the analysis of systems with multiple types of uncertainty representation. The QMU methodologies are then demonstrated on a stochastic model consisting of highly nonlinear analytical functions (Section V), a stochastic, multiphysics, spacecraft, reentry model (Section VI), and a multisystem model for the design and analysis of a high speed civil transport (Section VII.) These sections contain detailed information regarding the models, the stochastic problems, and the results of detailed QMU analyses. Lastly, a conclusion, summarizing the results, is given to tie up the findings of this work.

## II. Uncertainty Quantification Methodology

### A. Point-Collocation Nonintrusive Polynomial Chaos

In recent studies,<sup>10,11,13,15,16</sup> the polynomial chaos method has been used as a means of UQ over traditional methods, such as Monte Carlo, for its computational efficiency. Polynomial chaos is a stochastic method based on the spectral representation of the uncertainty. An important aspect of spectral representation of uncertainty is that a response value or random function  $\alpha^*$  can be decomposed into separable deterministic and stochastic components, as shown in Eq. (1).

$$\alpha^*(\mathbf{x}, \boldsymbol{\xi}) \approx \sum_{i=0}^P \alpha_i(\mathbf{x}) \Psi_i(\boldsymbol{\xi}) \quad (1)$$

Here,  $\alpha_i$  is the deterministic component and  $\Psi_i$  is the random variable basis functions corresponding to the  $i^{th}$  mode. It is assumed that  $\alpha^*$  is function of the deterministic, independent random variable vector  $\mathbf{x}$  and the  $n$ -dimensional standard random variable vector  $\boldsymbol{\xi}$ . Note that this series is, by definition, an infinite series. However, in practice, it is truncated and a discrete sum is taken over a number of output modes.<sup>14</sup> For a total order expansion,  $N_t$  terms are required, which can be computed from Eq. (2) for a polynomial chaos expansion (PCE) of order  $p$  and a number of random dimensions or variables,  $n$ .

$$N_t = P + 1 = \frac{(n + p)!}{n!p!} \quad (2)$$

Further details on polynomial chaos theory are given by Walters and Huyse<sup>17</sup> as well as Eldred.<sup>14</sup>

Polynomial chaos can be implemented using an intrusive or a non-intrusive approach. While an intrusive methods may appear straightforward in theory, for complex problems this process may be time consuming, expensive, and difficult to implement.<sup>10</sup> In contrast, the non-intrusive approach can be easily implemented to model the uncertainty propagation in complex computational simulations, since no modification to the deterministic model is required. The non-intrusive methods require only the response (or sensitivity<sup>18–20</sup> values at selected sample points to approximate the stochastic response surface.

Several methods have been developed for NIPC. Of these, the point-collocation NIPC method has been used extensively in many aerospace simulations and CFD problems.<sup>11,13,16,18</sup> The point-collocation method starts with replacing the uncertain variables with their polynomial expansions using Eq. (1). Then,  $N_t$  vectors are chosen in random space for a given PCE with  $N_t$  modes. The deterministic code is then evaluated at these points, which is the left hand side of Eq. (1). Following this, a linear system of  $N_t$  equations can be formulated and solved for the spectral modes of the random variables. This system is shown in Eq. (3).

$$\begin{pmatrix} \Psi_0(\xi_0) & \Psi_1(\xi_0) & \cdots & \Psi_P(\xi_0) \\ \Psi_0(\xi_1) & \Psi_1(\xi_1) & \cdots & \Psi_P(\xi_1) \\ \vdots & \vdots & \ddots & \vdots \\ \Psi_0(\xi_P) & \Psi_1(\xi_P) & \cdots & \Psi_P(\xi_P) \end{pmatrix} \begin{pmatrix} \alpha_0 \\ \alpha_1 \\ \vdots \\ \alpha_P \end{pmatrix} = \begin{pmatrix} \alpha^*(\mathbf{x}, \xi_0) \\ \alpha^*(\mathbf{x}, \xi_1) \\ \vdots \\ \alpha^*(\mathbf{x}, \xi_P) \end{pmatrix} \quad (3)$$

Note that for this linear system,  $N_t$  is the minimum number of deterministic samples required to obtain an analytical solution (i.e., the coefficient vector). If more samples are available and they are linearly independent, the system is considered overdetermined and can be solved using a least squares approach. The number of samples over the required minimum is represented by the use of an oversampling ratio (OSR), defined as the number of actual samples to the minimum number required (i.e.,  $N_t$ ). In general, the number of collocation points can be determined by multiplying Eq. (2) by an OSR. Hosder et al.<sup>12</sup> determined an effective OSR of 2 for the stochastic model problems studied as the accuracy of the PCE is dependent on the collocation point values.

### III. Types of Uncertainty and Mixed Uncertainty Propagation

#### A. Types of Uncertainty

Three main types of uncertainty exist in numerical modeling: aleatory uncertainty, epistemic uncertainty and numerical error.<sup>21</sup> Aleatory uncertainty is the inherent variation of a physical system. Such variation is due the random nature of input data and can be mathematically represented by a probability density function if substantial experimental data is available for estimating the distribution type. An example of this for stochastic CFD simulations could be the fluctuation in free-stream quantities. While still considered a random variable, these variables are not controllable and their uncertainty is sometimes referred to as irreducible. Epistemic uncertainty in a stochastic problem comes from several potential sources. These include a lack of knowledge or incomplete information of the behavior of a particular variable and ignorance or negligence with regards to accurate modeling of model parameters. Contrary to aleatory uncertainty, epistemic uncertainty is sometimes referred to as reducible uncertainty as an increase in knowledge regarding the physics of a problem, along with accurate modeling, can reduce the amount of this type of uncertainty. Epistemic uncertainty is typically modeled using intervals because the use of probabilistic distributions can lead to inaccurate predictions in the amount of uncertainty in a system. Upper and lower bounds of these intervals can be drawn from limited experimental data or from expert predictions and judgment.<sup>10,11</sup> The last type of error is numerical error. This is defined as a recognizable deficiency in any phase or activity of modeling and simulations that is not due to lack of knowledge of the physical system. Errors that are not well characterized must be considered to be epistemic uncertainties. In CFD, an example of this type of uncertainty would be the discretization error in both the temporal and spatial domains that comes from the numerical solution of the partial differential equations that govern the system.<sup>11</sup>

#### B. Mixed Uncertainty Quantification

Many stochastic problems, including those to be used in this study, may contain both epistemic and aleatory types of uncertainty. It is desirable to consider the contribution of both types of uncertainty simultaneously

by propagating this mixed uncertainty through the stochastic model. This can be done using a procedure known as second-order probability. The purpose of multi-step UQ described in the previous sections is to obtain an accurate NIPC response surface with computational efficiency. The NIPC response surface can then be used within second-order probability in place of the deterministic code, as shown in Figure 1. Second-order probability is a type of double loop sampling. In the outer loop, a vector of specific values for the epistemic variables is passed into the inner loop where the stochastic response surface resulting from the NIPC process is sampled for the single epistemic sample vector and every aleatory sample vector. The process is repeated for all of the epistemic sample vectors. This means that the total number of samples of the NIPC response surface is the number of epistemic samples times the number of aleatory samples. Each iteration of the outer loop generates a cumulative distribution function based on the aleatory uncertainty analysis in the inner loop. After completion of the process, what remains is a series of CDFs which, when plotted, gives intervals of the output variable from the model at different probability levels (i.e., p-box representation of mixed uncertainty output). This second-order probability can also be implemented with Monte Carlo approach that uses the original model in the place of the response surface, which is done for the first model problem in this study for comparison with the NIPC results.

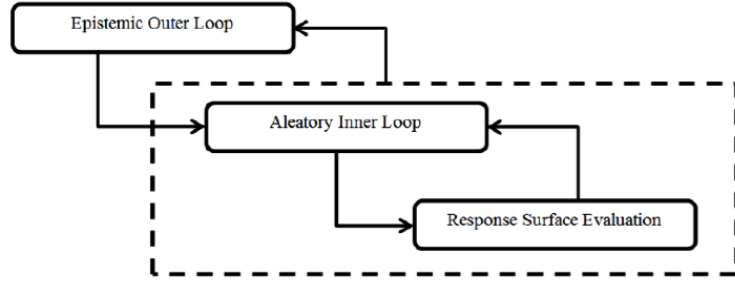


Figure 1: Schematic of Second-Order Probability

As shown by Eldred and Swiler,<sup>22</sup> the outer (epistemic) loop may also be replaced by optimization-based interval size determination approaches, which include both local and global optimization methods to determine interval bounds of the output response at selected probability levels. One approach, based on the combination of sampling and local optimization, can be utilized for the outer loop to determine the bounds at selected probability levels. The outer loop is first evaluated with a small number of samples to determine robust estimates for the initial values of epistemic variables used in local optimization. Then the optimization is performed with these initial starting points for minimizing or maximizing the response at selected probability levels. This approach provides a computationally efficient means of obtaining accurate results (i.e., interval bounds) via optimization without the cost of performing large sampling on the response surface in the outer loop.

## IV. Methodology for Quantification of Margins and Uncertainties

### A. Components of QMU

The key measures in the quantification of margins and uncertainties (QMU) are shown in Figure 2. In this QMU framework, for the whole aerospace system (spacecraft or aircraft) or for each sub-system, the first step will be to determine performance metrics (system outputs) relevant to the systems modeling. Then, these metrics will be evaluated at a design condition (point) determined for safe and reliable operation of the aerospace system. Each of these metrics ( $\mathbf{F}$ ) will typically involve some amount of uncertainty ( $U_F$ ) due to the inherent (aleatory) or real-life variation of parameters used in physical models, as well as epistemic uncertainties. The safe and reliable operation region of the performance metrics (performance gates) may be bounded with a lower ( $FL$ ) and/or an upper bound ( $FU$ ) for each metric, which may also include some uncertainty ( $U_{FL}$  for  $FL$  and  $U_{FU}$  for  $FU$ ) due to the aforementioned uncertainty sources. A measure of the distance between the design value of each performance metric and the lower boundary including the effect of uncertainties  $U_F$  and  $U_{FL}$  will give the lower margin  $M_{LW}$  and the distance between the upper boundary and the design value of each performance metric including the effect of uncertainties  $U_F$  and  $U_{FU}$  will give the upper margin  $M_{UP}$ .

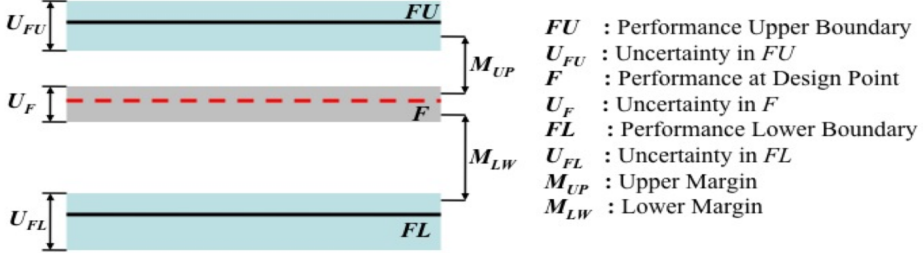


Figure 2: Schematic of Key Measures used in a QMU Analysis

Using the uncertainty and the margin information, a metric has to be developed to quantify and certify the confidence in safe operation of a system with a given performance metric. A confidence ratio ( $CR$ ) can be defined as shown in Eq. (4). The confidence ratio is obtained as the minimum of the ratio of the margin to the uncertainty calculated for each side of a performance metric. For a system wide confidence level, the minimum of the  $CRs$  is utilized to represent the most critical or unreliable component of the system. Note that it is not always required that a performance metric possess both an upper and a lower performance boundary. In fact, it may be the case of many engineering applications that only a single limit may bound a performance metric. In this case, only a single ratio of the margin to the uncertainty exists and is considered as the confidence ratio for that particular metric (i.e. system performance or output.)

$$CR = \text{Min} \left[ \frac{M_{UP}}{U_{UP}}, \frac{M_{LW}}{U_{LW}} \right] \quad (4)$$

## B. Uncertainty Calculations

In order to measure the uncertainty in the performance gate(s) of a system, the first step is to perform the actual uncertainty quantification of the design and the performance limits. In many problems, stochastic models may be used for determining the uncertainty in the output based on random input variables. This can be done by various UQ propagation methods; however, it is one of the goals of the current study to use stochastic responses surfaces for their computational efficiency and accuracy (see section II.) It may also be the case that models are not directly available and the uncertainty must be quantified by other means. One example could be the use experimental test data. Then, it may be possible to represent the uncertainty of a design or performance limit with an interval or possibly fit a distribution to the data depending on its behavior.

After quantifying the uncertainty in the design and the performance limits, the next step is to quantify the uncertainty in the performance gates. For a probabilistic representation of the uncertainty, one approach would be to use Eqs. (5) and (6).

$$U_{UP} = \sqrt{\left( (FU_{max})_{P=0.5} - (FU_{min})_{P=\frac{1-\beta}{2}} \right)^2 + \left( (F_{min})_{P=0.5} - (F_{max})_{P=\frac{1+\beta}{2}} \right)^2} \quad (5)$$

$$U_{LW} = \sqrt{\left( (FL_{max})_{P=0.5} - (FL_{min})_{P=\frac{1-\beta}{2}} \right)^2 + \left( (FL_{min})_{P=0.5} - (FL_{max})_{P=\frac{1+\beta}{2}} \right)^2} \quad (6)$$

Here,  $\beta$  represents the confidence level used in the analysis and  $P$  represents the probability level at which the functional values are taken. For example, if  $\beta = 0.95$ , this would correspond to a 95% confidence level analysis. In case of mixed uncertainty in  $F$ ,  $FU$ , and/or  $FL$ , min corresponds to the minimum and the max corresponds to maximum response value (bound) of the interval at that particular probability level, which can be obtained from the probability-box of the associated responses. Each of the square terms represents the uncertainty in either the design or a performance limit. Notice that the entire range of uncertainty in the design and the performance limits are not considered in Eqs. (5) and (6). By including only the uncertainty that will directly effect the performance gate on each side, the amount of uncertainty is restricted to each of the performance gates to avoid the under prediction of the reliability of the system as given by the CR in Eq. (4). For example, the uncertainty in the upper performance gate is measured by roughly the upper half of the uncertainty in the design and the lower half of the uncertainty in the upper performance limit. Similarly

for the lower performance gate, the uncertainty is measured by roughly the lower half of the uncertainty in the design and the upper half of the uncertainty in the lower performance limit. In the case of mixed uncertainty, a conservative approach is taken to assess the amount of uncertainty in the performance gates. From Eq. (5), for example, the uncertainty in the design is measured as the distance between the upper output value at a selected probability level and the lower output value at the 50% probability level. Notice that the ladder of the two values is taken further from the performance gate in order to ensure that any uncertainty that could affect the reliability of the system is included in the measurement of the amount of uncertainty in the performance limit.

It is desirable to generalize the uncertainty measurements in Eqs. (5) and (6) to include non-probabilistic representation of the uncertainty. This is done with Eqs. (7) and (8) where each of the terms are defined, based on the representation of the uncertainty, in Tables 1 and 2 for the upper and lower performance gates, respectively.

$$U_{UP} = \sqrt{(U_{UP1} - U_{UP2})^2 + (U_{UP3} - U_{UP4})^2} \quad (7)$$

$$U_{LW} = \sqrt{(U_{LW1} - U_{LW2})^2 + (U_{LW3} - U_{LW4})^2} \quad (8)$$

**Table 1: Response Values of Different Uncertainty Representations for Upper Uncertainty Calculations**

Uncertainty Representation	$U_{UP1}(FU)$	$U_{UP2}(FU)$	$U_{UP3}(F)$	$U_{UP4}(F)$
No Uncertainty	$FU$	$FU$	$F$	$F$
Pure Epistemic	$\frac{FU_{max}}{2}$	$\frac{FU_{min}}{2}$	$\frac{F_{max}}{2}$	$\frac{F_{min}}{2}$
Pure Aleatory	$(FU)_{P=0.5}$	$(FU)_{P=\frac{1-\beta}{2}}$	$(F)_{P=\frac{1+\beta}{2}}$	$(F)_{P=0.5}$
Mixed	$(FU_{max})_{P=0.5}$	$(FU_{min})_{P=\frac{1-\beta}{2}}$	$(F_{max})_{P=\frac{1+\beta}{2}}$	$(F_{min})_{P=0.5}$

**Table 2: Response Values of Different Uncertainty Representations for Lower Uncertainty Calculations**

Uncertainty Representation	$U_{LW1}(FL)$	$U_{LW2}(FL)$	$U_{LW3}(F)$	$U_{LW4}(F)$
No Uncertainty	$FL$	$FL$	$F$	$F$
Pure Epistemic	$\frac{FL_{max}}{2}$	$\frac{FL_{min}}{2}$	$\frac{F_{max}}{2}$	$\frac{F_{min}}{2}$
Pure Aleatory	$(FL)_{P=0.5}$	$(FL)_{P=\frac{1+\beta}{2}}$	$(F)_{P=\frac{1-\beta}{2}}$	$(F)_{P=0.5}$
Mixed	$(FL_{min})_{P=0.5}$	$(FL_{max})_{P=\frac{1+\beta}{2}}$	$(F_{min})_{P=\frac{1-\beta}{2}}$	$(F_{max})_{P=0.5}$

### C. Margin Calculations

Calculation of the distance between the design condition and the performance limit, or the margin, is a critical component of QMU. Improper measurement could result in under or over prediction of the reliability of the system. While this measurement may graphically appear obvious as seen in Figure 2, if both the design and the performance limits possess uncertainty, the calculations should include the effects of these uncertainties to obtain an accurate margin estimate. Moreover, a general approach has been devised since the uncertainty characteristics (aleatory, epistemic, or mixed) for the design and limits may be different. Considering these, the calculation of the margins for a probabilistic representation of the uncertainty can be determined using Eqs. (9) and (10) for the upper and lower performance boundaries, respectively.

$$M_{UP} = \left| (FU_{min})_{P=\frac{1-\beta}{2}} - (F_{max})_{P=\frac{1+\beta}{2}} \right| \quad (9)$$

$$M_{LW} = \left| (F_{min})_{P=\frac{1-\beta}{2}} - (F_{Lmax})_{P=\frac{1+\beta}{2}} \right| \quad (10)$$

Here,  $\beta$  represents the confidence level used in the analysis and  $P$  represents the probability level at which the functional values are taken. For example, if  $\beta = 0.95$  this would correspond to a 95% confidence level analysis.

If the distribution of the performance metric and/or the design limits are known (e.g. Gaussian) these values can be easily obtained from the statistics of the distribution. In general, the distribution of a system or model output is almost never known exactly, even when the inputs are on clearly defined distributions. In this case, response values may be obtained from a cumulative distribution function (CDF) formulation of the output. This is the typical approach when considering problems under a pure aleatory analysis or under mixed uncertainty where the outputs carry some probabilistic representation. Note also that the "min" and "max" subscripts in Eqs. (9) and (10) indicate the response value that should be selected when multiple response values exist at a single probability level. For instance, this occurs when a model or system is subject to mixed uncertainty as mentioned in section III. B. which creates a range of values at each probability level defined by multiple CDFs (i.e., the CDFs that form the probability-box.)

Another type of uncertainty representation of either the design or the limits may be the non-probabilistic or pure epistemic representation. In this case, there is no distribution of the output and the uncertainty is only defined by an interval. Here the approach is to use the interval bounds as the measurement point for determining the margins rather than a response value defined at a specific probability level, which is not possible in this case. Note that this will be the most conservative approach and may be warranted given the unknown behavior of the uncertainty of epistemic intervals.

One of the objectives of this study is to demonstrate how a QMU analysis can be performed when the output uncertainty of design points and operational limits are different. The three possibilities include pure epistemic (interval), pure aleatory, and mixed uncertainty. Eqs. (9) and (10) can be generalized to Eqs. (11) and (12), where each term is based on the representation of the uncertainty of the specific component of the system. The possible values of the  $M_{UP}$  and  $M_{LW}$  are summarized in Table 3.

$$M_{UP} = |M_{UP1} - M_{UP2}| \quad (11)$$

$$M_{LW} = |M_{LW1} - M_{LW2}| \quad (12)$$

**Table 3: Response Values of Different Uncertainty Representations for Margin Calculations**

Uncertainty Representation	$M_{UP1}(FU)$	$M_{UP2}(F)$	$M_{LW1}(F)$	$M_{LW2}(FL)$
No Uncertainty	$FU$	$F$	$F$	$FL$
Pure Epistemic	$FU_{min}$	$F_{max}$	$F_{min}$	$FL_{max}$
Pure Aleatory	$(FU)_{P=\frac{1-\beta}{2}}$	$(F)_{P=\frac{1+\beta}{2}}$	$(F)_{P=\frac{1-\beta}{2}}$	$(FL)_{P=\frac{1+\beta}{2}}$
Mixed	$(FU_{min})_{P=\frac{1-\beta}{2}}$	$(F_{max})_{P=\frac{1+\beta}{2}}$	$(F_{min})_{P=\frac{1-\beta}{2}}$	$(FL_{max})_{P=\frac{1+\beta}{2}}$

## V. Analytical QMU Model Problem

To demonstrate the quantification of margins and uncertainties using stochastic expansions with various uncertainty representation types in the design points and performance limits, an analytical model problem was selected. This model consists of a complex system of highly nonlinear functions typically used as test functions in numerical optimization studies. The objective with this model is to demonstrate both the UQ and QMU approaches described in the previous sections on a general problem where two non-linear systems are coupled, share common input variables, and both performance metrics and system boundaries have different uncertainty characteristics (i.e., pure aleatory, epistemic, or mixed). The following sections outline the deterministic model as well as the stochastic model. Then, both UQ and QMU are performed with a detailed description of the processes and the results.

## A. Description of the Deterministic Model

### 1. Design

The deterministic model is shown in Figure 3. This model consists of two primary systems including two outputs or performance metrics. Each system is made up of a nonlinear, analytical function. The first is the multivariate form of the Rosenbrock function and the second is known as the McCormick function. Notice also the dependence of system 2 on the output of system 1.

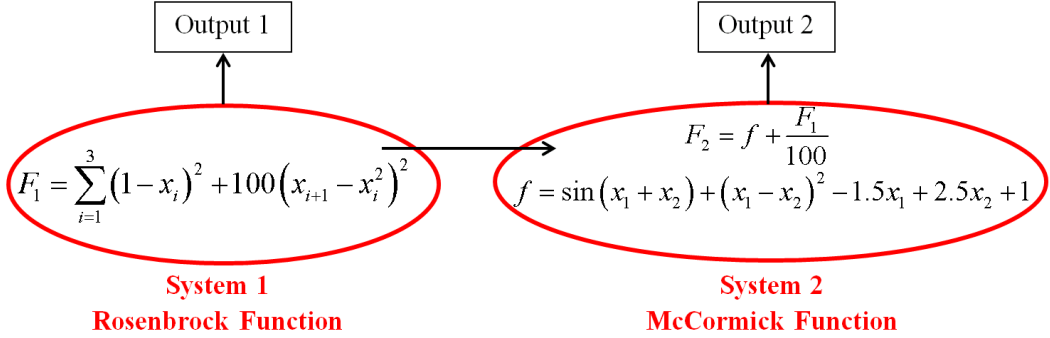


Figure 3: System Design Schematic for the Analytical Model Problem

### 2. Performance Limits

The output of system 1 is constrained by both an upper and a lower performance limit. The upper limit is comprised of its own model, shown in Eq. (13).

$$FU_1 = (y_1 + 2x_1 - 7)^2 + (2y_1 + x_1 - 5)^2 \quad (13)$$

This function is known as the Booth function. Notice that one of the variables in this function is the same as one of the variables in the system design. This adds a degree of complexity to the overall system. The lower limit is, however, not governed by a model, but rather is made up of statistical data. The second system is only bounded on the upper side. In this case, the uncertainty in the performance limit is represented by an epistemic interval.

## B. Description of the Stochastic Model

### 1. Design

The design condition model consists of four input uncertain parameters. Two are represented by pure epistemic intervals and two are aleatory variables with uniform distributions, indicating that the model design output (performance metric) will involve mixed uncertainty. These variables are shown in Table 4.

Table 4: Uncertain Input Parameters for the Analytical Model Performance Metrics

Variable	Distribution	Mean/lower boundary	Std/upper boundary
$x_1$	Epistemic	-1.0	1.0
$x_2$	Uniform	-0.5	0.4
$x_3$	Uniform	-0.6	0.7
$x_4$	Epistemic	-0.5	1.0

## 2. Performance Limits

As stated above, the upper boundary on the system 1 performance limits is defined by the model in Eq. (13). This model is made up of two uncertain variables, shown in Table 5. Notice again that one of the variables is the same as one from the design condition of the system.

The lower limit for system 1 is assumed to be made up of purely statistical data. This data is represented by a Gaussian distribution with a mean of -10.0 and a standard deviation of 0.1. Lastly, the uncertainty in the upper limit of system 2 is represented by an epistemic interval given by [15.0, 17.0]. A summary of the performance limit uncertainty information is given in Table 5.

**Table 5: Uncertain Input Information for System 1 and System 2 Performance Limits**

Variable	Distribution	Mean/lower boundary	Std/upper boundary
$FU_1$ Input $y_1$	Gaussian	25.0	2.0
$FU_1$ Input $x_1$	Epistemic	-1.0	1.0
$FL_1$	Gaussian	-10.0	0.1
$FU_2$	Epistemic	15.0	17.0

## C. Uncertainty Quantification

### 1. Design

Performing the UQ on the performance metrics and the performance limits is next step in the analysis. For system 1 of the design, a stochastic response surface could be formulated using a forth order polynomial chaos expansion. With four uncertain variables, a total number of 70 evaluations of the deterministic model were required using an OSR of 2. The results are compared to a Monte Carlo (MC) simulation using the sampling/optimization approach in the epistemic loop of second-order probability described in Section III C., which required 2074 evaluations of the deterministic model (optimization performed at 15 probability levels.) The upper and lower CDFs of the output P-Box are given in Figure 4, which also indicates the accuracy of the NIPC response surface when compared to MC.

For system 2 of the design, a stochastic response surface could be formulated using a forth order polynomial chaos expansion. With four uncertain variables, a total of 70 evaluations of the deterministic model were required using an OSR of 2. The results are compared to a Monte Carlo simulation using the sampling/optimization approach in the epistemic loop of second-order probability described in Section III C., which required 1675 evaluations of the deterministic model (optimization performed at 15 probability levels.) The upper and lower CDFs of the output P-Box are given in Figure 5, which also shows a great agreement between NIPC and MC results.

### 2. Performance Limits

Similar to the design of the system, the uncertainty in the upper performance limit of system 1 was represented by a second order polynomial chaos expansion. This required only 12 evaluations of the deterministic model using an OSR of 2. A comparison with Monte Carlo is shown in Figure 6 depicting the upper and lower CDFs of the output. Note that a total number of 61 evaluations of the deterministic model were required for the combined sampling/optimization Monte Carlo analysis (optimization performed at 15 probability levels.)

The uncertainty in the two other performance limits are already specified as there is no model used to determine the output. For the lower performance limit of system 1, the uncertainty is represented by a Gaussian distribution with a mean of -10.0 and a standard deviation of 0.1. The upper limit on system 2 is represented by an epistemic interval ranging from 15.0 to 17.0.

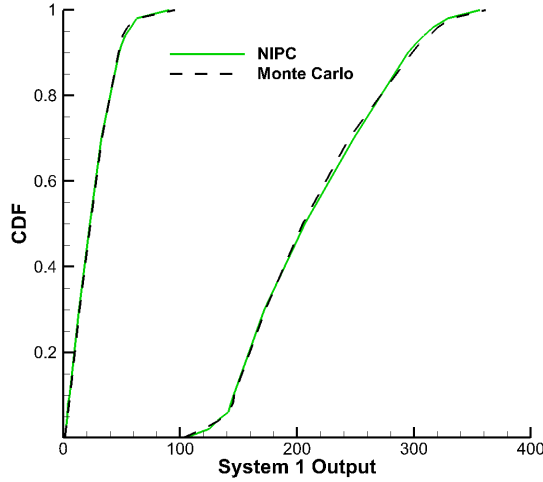


Figure 4: System 1 Output P-Box Plot

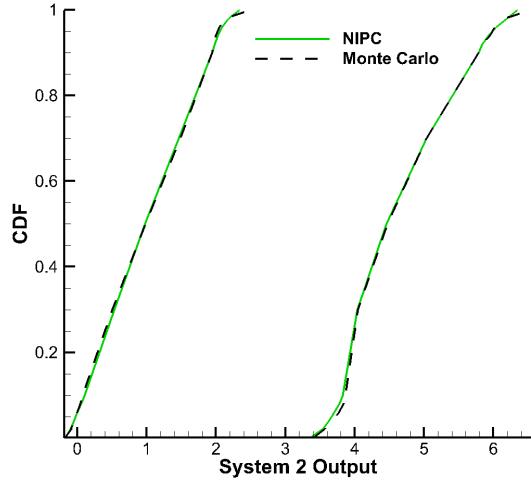


Figure 5: System 2 Output P-Box Plot

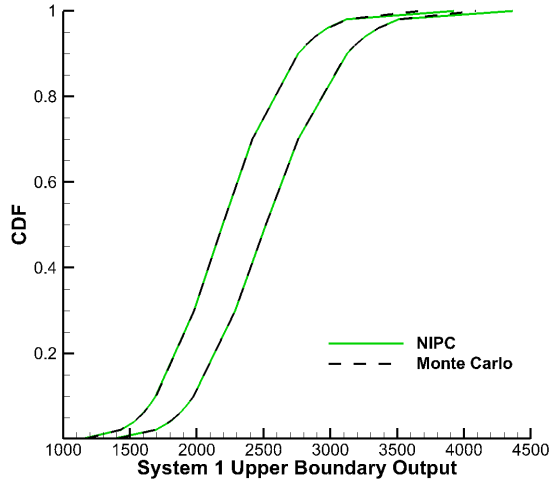


Figure 6: P-box Plot of the Output of System 1 Upper Boundary

#### D. Quantification of Margins and Uncertainties

After obtaining the uncertainty in the components of the system, it is now possible to perform the QMU analysis. A 95% confidence analysis (i.e.,  $\beta = 0.95$ ) has been selected for this problem. Using the equations and tables given in section IV. B., the margin and performance gate uncertainty calculations can be performed. For system 1, both the design and the upper performance limit are represented by mixed uncertainty, while the lower limit is a pure aleatory representation. A summary of the margin and performance gate uncertainty values are given in Table 6 as well as the resulting confidence ratios of the system. Note that the minimum of these two confidence ratios is deemed the confidence ratio of system 1. For clarity, the margin and uncertainty measurements are shown in Figure 7.

Similarly, the QMU analysis is performed on system 2. Here, the design is represented by mixed uncertainty while the only performance limit, located on the upper side of the performance metric, is represented by an epistemic interval. A summary of the margin and performance gate uncertainty values are shown in Table 7 as well as the resulting confidence ratio of the system.

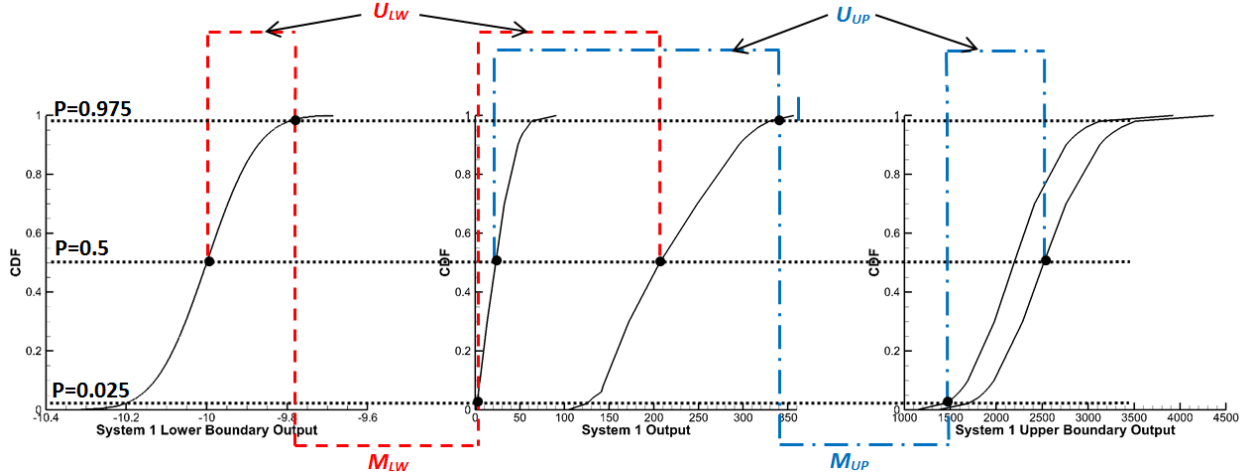


Figure 7: QMU Margin and Uncertainty Measurements for System 1

Table 6: System 1 QMU Analysis Metrics

Performance Gate	Margin	Uncertainty	CR
Lower	12.41	217.51	0.057
Upper	1119.65	1111.04	1.008

There are two resulting confidence ratios from the QMU analysis, one from each system. A system wide confidence level would then be the minimum of these two ratios which is shown to be 0.057. This value indicates very poor confidence in the reliability of the system as the uncertainty in the performance gate between the design and the lower performance limit is significantly larger than the margin. From a practical standpoint, this would indicate that a re-analysis/design of the system, the performance limit, or both may be necessary to improve the reliability of the system.

Table 7: System 2 QMU Analysis Metrics

Performance Gate	Margin	Uncertainty	CR
Upper	8.84	5.28	1.67

## VI. Spacecraft Reentry QMU Model Problem

To further demonstrate the quantification of margins and uncertainties using stochastic expansions with various uncertainty representations between the design points and performance limits, a second aerospace model problem is chosen, which is a multisystem, physics based model for atmospheric, lifting entry of a spacecraft. Systems within the design include a model for six-degree of freedom reentry dynamics used for the determination of a reentry trajectory. The second system is a prediction model of stagnation point, convective heat flux used to determine the maximum heat load experienced along the reentry trajectory. In this problem, a generic planetary entry capsule similar to Crew Exploration Vehicle (CEV) was analyzed for a lunar return mission.<sup>23-25</sup> The purpose of this model is demonstrate the QMU of a coupled, multisystem design possessing mixed uncertainty, as well as performance boundaries with different types of uncertainty representation.

### A. Description of the Deterministic Model

#### 1. Design

The deterministic model is shown in the system diagram in Figure 8. This model consists of two primary systems with three outputs or performance metrics.

The first system has two primary components or subsystems. The first of these is the trajectory model consisting of a six degree of freedom model for atmospheric entry of a lifting body. The kinematics are shown in Eqs. (14) through (17) and the equations of the dynamical system are shown in Eqs. (18) through (20).<sup>26,27</sup>

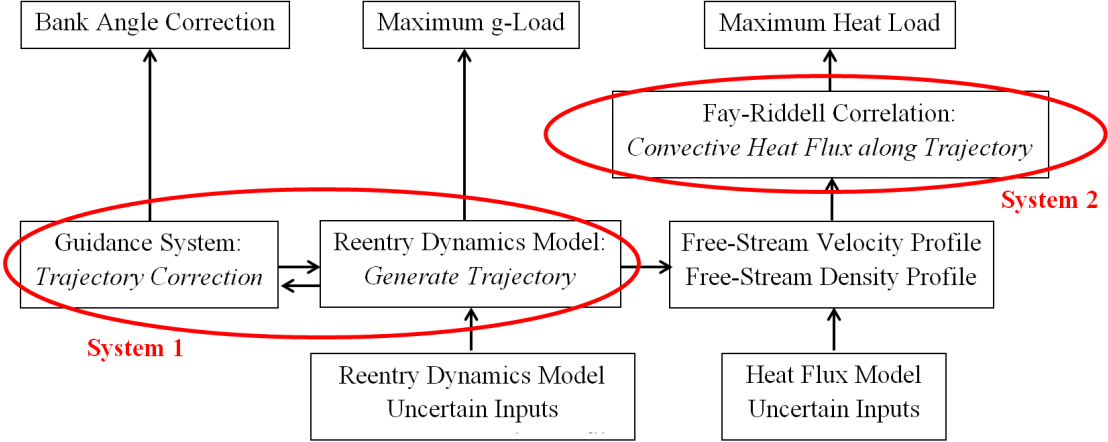


Figure 8: System Design Schematic for the Spacecraft Reentry Model Problem

$$\frac{dr}{dt} = V \sin \gamma \quad (14)$$

$$\frac{d\phi}{dt} = \frac{V \cos \gamma \cos \psi}{r} \quad (15)$$

$$\frac{d\theta}{dt} = \frac{V \cos \gamma \sin \psi}{r \cos \phi} \quad (16)$$

$$\frac{ds}{dt} = V \cos \gamma \quad (17)$$

$$\frac{dV}{dt} = -\frac{D}{m} - g \sin \gamma + \omega^2 r \cos \phi (\sin \gamma \cos \phi - \cos \gamma \sin \phi \cos \psi) \quad (18)$$

$$V \frac{d\gamma}{dt} = \frac{L}{m} \cos \sigma - g \cos \gamma + \frac{V^2}{r} \cos \gamma + 2\omega V \cos \phi \sin \psi + \omega^2 r \cos \phi (\cos \gamma \cos \phi + \sin \gamma \sin \phi \cos \psi) \quad (19)$$

$$V \frac{d\psi}{dt} = \frac{L \sin \sigma}{m \cos \gamma} + \frac{V^2}{r} \cos \gamma \sin \psi \tan \phi - 2\omega V (\tan \gamma \cos \phi \cos \psi - \sin \phi) + \frac{\omega^2 r}{\cos \gamma} \sin \phi \cos \phi \sin \psi \quad (20)$$

In this system,  $V$  is velocity,  $m$  is mass,  $D$  is drag,  $L$  is lift,  $r$  is the orbital radius,  $\gamma$  is the flight path angle,  $\theta$  is the longitude,  $\phi$  is the latitude,  $\sigma$  is the bank angle,  $\omega$  is the planetary body rotational speed,  $\psi$  is the heading angle, and  $s$  is the range. This is a system of 7 ordinary differential equations that can be numerically integrated simultaneously in time. An example trajectory for a typical lunar return skip reentry mission is shown in Figure 9.

The second component of this system is a guidance system, coupled to the primary reentry trajectory model. The guidance system is used to correct the trajectory in the instance of deviation from a nominal trajectory, such as when the reentry is subject to perturbation or uncertainty. In order to correct the trajectory, the guidance system uses a search algorithm to modify the bank angle of the trajectory. This effectively changes the direction of the lift vector in order to steer the spacecraft towards a target landing location. In this model problem, the reentry trajectory begins with the bank angle on the nominal value for the baseline trajectory. A single bank angle correction is performed when a sensible atmosphere is detected which occurs approximately when the g-load reaches a value of 0.05.<sup>28</sup> The necessary bank angle correction is determined using a simple root finding method, shown in Eq. (21) for the  $i^{th}$  step in the search. The search is based on the distance between the target location and the projected landing location at the current bank angle shown in Eq. (22), which is only a function of the bank angle as no other control is being simulated.

$$\sigma_i = \sigma_{i-1} - \frac{\sigma_{i-1} - \sigma_{i-2}}{f(\sigma_{i-1}) - f(\sigma_{i-2})} f(\sigma_{i-1}) \quad (21)$$

where,

$$f(\sigma) = s_{miss} = s_{current} - s_{target} \quad (22)$$

Here,  $s_{current}$  is the range traveled with the current bank angle obtained from integrating the above dynamical system and  $s_{target}$  is the range to the target from the projected landing location measured as a greater circle distance. Once the optimum bank angle is determined, the baseline bank angle is corrected instantaneously and the remainder of the trajectory is carried out.

In the reentry dynamics system, there are a total of two outputs. The first is the maximum g-load experienced along the trajectory. This is a critical trajectory and vehicle design value as it directly influences the safety of the crew as well as the structural loads that the vehicle may experience. The second output is the required bank angle correction. This value may be critical in the design of an adequate reaction control system including propulsive capabilities and propellant requirements.<sup>29</sup>

The second system in this model is a model for the stagnation point, convective, heat flux of a blunt body in hypersonic flow. The Fay and Riddell<sup>30</sup> correlation was used to approximate the stagnation point heat transfer for a blunt body in hypersonic flow. This model assumes a laminar boundary layer, thermo-chemical equilibrium flow, and a fully catalytic wall. The model is shown in Eq. (23).

$$\dot{q}_w = 0.76(Pr^{-0.6})(\rho_w \mu_w)^{0.1}(\rho_e \mu_e)^{0.4} \sqrt{\frac{du_e}{dx}} (h_{0e} - h_w) \left( 1 + (Le^{0.52} - 1) \frac{h_D}{h_{0e}} \right) \quad (23)$$

where,

$$\frac{du_e}{dx} = \frac{1}{R_n} \sqrt{\frac{2(P_e - P_\infty)}{\rho_e}} \quad (24)$$

$$h_D = \sum_i c_i (h_f^0)_i \quad (25)$$

In the above equations,  $Pr$  is the Prandtl number,  $Le$  is the Lewis number,  $R_n$  is the radius of curvature of the body,  $h_D$  is the dissociation enthalpy,  $c_i$  is the mass fraction of the atomic species within the boundary layer, and  $(h_f^0)_i$  is heat of formation of atomic species  $i$ . Note also that the subscripts  $w$  and  $e$  represent the wall and boundary layer edge quantities, respectively. For this problem, a boundary condition at the wall is necessary to close the problem as fluid properties at the wall are required. A radiation, adiabatic wall condition was assumed. This implies that the wall temperature is not fixed, but the heat flux through the wall is zero (i.e. the heat transfer to the wall from the fluid due to conduction and diffusion must equal the heat transfer radiated away from the surface.) Mathematically this is shown with Eq. (26).

$$\dot{q}_r = \dot{q}_d + \dot{q}_c = \dot{q}_w \quad (26)$$

where,

$$\dot{q}_r = \epsilon \sigma T_w^4 \quad (27)$$

Here,  $\dot{q}_d$  is the heat transfer due to diffusion,  $\dot{q}_c$  is the heat transfer due to conduction,  $\epsilon$  is the wall emissivity and  $\sigma$  is the Stefan-Boltzmann constant. Note that the heat transfer due to the radiation from

the shock layer has been neglected. For given free stream conditions, the flow properties behind the standing bow shock along the stagnation streamline can be calculated using an equilibrium shock calculation procedure outlined in Anderson.<sup>31</sup> It can be assumed that the properties directly behind the shock are the properties on the edge of the boundary layer. The boundary layer edge viscosity is calculated using Sutherlands law. The pressure at the wall can be assumed to be the pressure at the boundary layer edge. Finally, the last step is to find the remaining properties at the wall; however, these are unknown because wall temperature is not specified. This requires then that Eqs. (23) and (26) be solved simultaneously with the system being implicitly dependent on the wall enthalpy (found using high temperature equilibrium polynomial curve fits from Tannehill et al.<sup>32</sup>), wall viscosity (from Sutherlands Law) and the wall density (from the equation of state.) A simple root finding method can be implemented to resolve the system. The solution of the system then gives the radiative, adiabatic wall temperature at which the convective heat flux to the wall is radiated away from the surface.

It is important to note the coupling between the reentry dynamics of system 1 and the aerothermodynamics of system 2. The heat flux is calculated at multiple points along the trajectory in order to locate the maximum value. Note that calculations are not performed when the continuum flow assumption is no longer valid (altitude greater than approximately 100 km) and when the flow is no longer supersonic. These conditions violate the assumptions of the model. However, the maximum heat flux would not occur in these regions so there is no possible loss of accuracy in capturing the maximum heat load.

## 2. Performance Limits

For system 1, performance limits exist for both outputs. The maximum g-load is constrained by the limits the crew and the structure of the spacecraft can withstand meaning that only an upper limit exists. In order to represent this limit, an epistemic interval has been utilized. The performance limits of the bank angle correction would be based on the control and propellant limitations of the spacecraft. In this study, the upper and lower limits are firm boundaries, with no uncertainty. For system 2, there is only an upper limit on the heat flux as any lower limit would not be a concern. In this case, the upper limit was represented by an epistemic interval. This interval was selected to reflect the physical limitations of current TPS materials.

## B. Description of the Stochastic Model

### 1. Design

In system 1 there is a total of 10 uncertain variables, both coming from epistemic and aleatory sources. Epistemic sources include entry interface (E.I.) altitude, mass, drag coefficient and lift coefficient. Aleatory sources include E.I. velocity, E.I. flight path angle, the reference area, E.I. latitude, E.I. longitude, and E.I. heading angle. The uncertainty in these parameters and their distribution are shown in Tables 8. Note that many of the selected uncertain parameters and classification are consistent with previous uncertainty work in this area.<sup>23, 24, 26, 27</sup>

For system 2, 10 variables were selected as sources of uncertainty. Both epistemic (model form) and aleatory (inherent) forms of uncertainty were considered. The epistemic uncertain variables were as follows: Lewis number, Prandtl number, boundary layer edge viscosity, emissivity, the heats of formation for nitrogen and oxygen and the power over the Lewis number. These model variables are considered as epistemic by imposing uncertainty on them due to lack of knowledge. Note that uncertainty in the two heats of formation and the boundary layer edge viscosity were modeled through the introduction of a factor,  $k$ , to each variable, which was used to represent a variation in the uncertain variable (e.g.  $x = k (x_{ref})$ .) The factor  $k$  for each variable was treated as an epistemic uncertain variable. The other three variables were treated as aleatory (inherent) uncertain variables: free stream velocity, free stream density, and the radius of curvature of the body. Random fluctuations in the free-stream conditions are possible during flight and variations in the vehicle geometry are possible due to manufacturing processes. These variables were assumed normally distributed about some mean with a coefficient of variance (CoV) of 1%. The input uncertainties for each of the uncertain variables are summarized in Table 9.

**Table 8: Reentry Model Uncertain Parameters for System 1**

Variable	Distribution	Mean/ Min	Std./ Max
E.I. $h$ , m	Epistemic	121800	122000
$m$ , kg	Epistemic	9000	9500
$C_D$	Epistemic	1.27	1.31
$C_L$	Epistemic	0.367	0.407
E.I. $U_\infty$ , m/s	Gaussian	10900	30.0
E.I. $\gamma$ , deg.	Uniform	-6.1	-5.9
$S$ , m <sup>2</sup>	Gaussian	19.9	0.2
E.I. $\phi$ , deg.	Gaussian	0.0	1.0
E.I. $\theta$ , deg.	Gaussian	0.0	1.0
E.I. $\psi$ , deg.	Gaussian	0.0	1.0

**Table 9: Reentry Model Uncertain Parameters for System 2**

Variable	Distribution	Mean/ Min	Std./ Max
$Le$	Epistemic	1.358	1.442
$Pr$	Epistemic	0.679	0.721
$\mu_e$ Factor	Epistemic	0.97	1.03
$\epsilon$	Epistemic	0.776	0.824
$h_f^0$ (N) Factor	Epistemic	0.97	1.03
$h_f^0$ (O) Factor	Epistemic	0.97	1.03
Power on $Le$	Epistemic	0.5044	0.5356
$U_\infty$ Factor	Gaussian	1.0	0.01
$\rho_\infty$ Factor	Gaussian	1.0	0.01
$R_n$ , m	Gaussian	6.93	0.0693

## 2. Performance Limits

For system 1, the upper performance limit is represented by an epistemic interval as stated in the previous section. The g-load limit was selected to be on the interval [10, 11] g. Also for system 1, the limitations of the bank angle correction are defined as boundaries with no uncertainty. The boundaries were elected to be  $\pm 20$  deg. For system 2, the epistemic interval was selected to be [900, 1200] W/cm<sup>2</sup>. The uncertainty in this interval was extrapolated from several sources indicating different heat load values of the stardust mission including CFD simulations as well as sensor data collected during flight.<sup>33-35</sup>

## C. Uncertainty Quantification

### 1. Design

Performing the UQ in the system design condition and the performance limits is the next step in the analysis. From the previous section, there is a total of 20 uncertain parameters in this model problem. Using Eq. (2), 462 evaluations of the deterministic model were required for an OSR=2 with second order polynomial chaos expansions. The upper and lower CDFs of the output P-Boxes are given in Figures 10 and 11 for the g-load and bank angle correction, respectively. Note that these were obtained using the sampling approach for mixed uncertainty outlined in section III.C.

A similar analysis was performed on system 2 of the design. A stochastic response surface could be formulated using a second order polynomial chaos expansion. The upper and lower CDFs of the output P-Box are given in Figure 12, which were obtained using the sampling approach for mixed uncertainty outlined in section III.C.

In the previous model problem, a comparison of Monte Carlo and NIPC results was made in order to confirm the accuracy of the NIPC response surfaces. This was possible because of the low computational cost of the model. The reentry dynamics model is significantly more computationally expensive making an accurate Monte Carlo solution infeasible to obtain. However, it is still possible to check the accuracy of the surrogate model by comparing results obtained from the actual model to those obtained from the surrogate model at the same sample location in the design space. In this study, 20 sample points, distributed evenly in the design space, were used to measure the accuracy of the surrogate models. Of the three surrogates created in this model problem, the highest mean error in the sample points was about 0.2% validating the selection of second order polynomial chaos expansions. Note that these sample points differ from the sample points used to train the surrogate model.

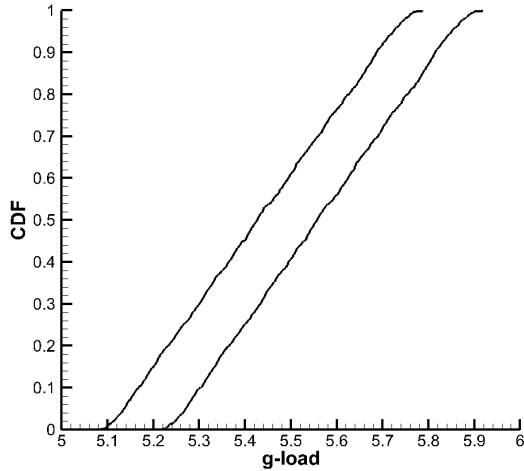


**Figure 10: Maximum g-Load P-Box Plot from System 1**

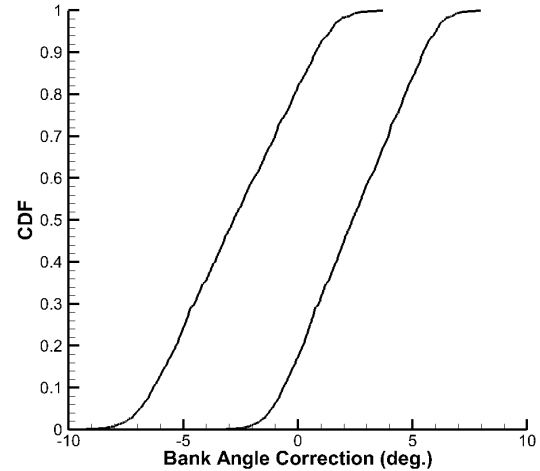


**Figure 11: Bank Angle Correction P-Box Plot from System 1**

## 2. Performance Limits

No uncertainty quantification was performed on the performance limits for this model as both models were assigned epistemic intervals or boundaries with no uncertainty.

### D. Quantification of Margins and Uncertainties

After assessing the uncertainty in the components of the system, it is now possible to perform the QMU analysis. A 95% confidence analysis (i.e.,  $\beta = 0.95$ ) has been selected for this problem. Using the equations and tables given in section IV. B., the margin calculations can be performed. For system 1, both the design metrics are represented by mixed uncertainty. The upper performance limit of the maximum g-load was represented by an epistemic interval while the upper and lower bounds of the bank angle correction were fixed values with no uncertainty. A summary of the margin and performance gate uncertainty values as well as the resulting confidence ratios of the system are given in Tables 10 and 11. Note that the minimum of these two confidence ratios is deemed the confidence ratio for the system.

**Table 10: Maximum g-Load QMU Analysis Metrics from System 1**

Performance Gate	Margin	Uncertainty	CR
Upper	4.13	0.67	6.17

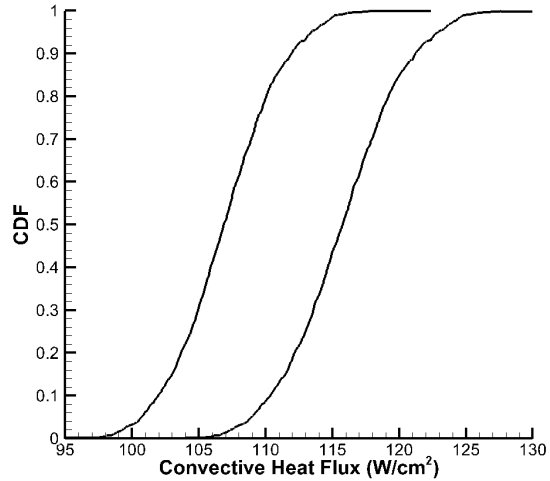


**Figure 12: Maximum Heat Load P-Box Plot from System 2**

**Table 11: Bank Angle Correction QMU Analysis Metrics from System 1**

Performance Gate	Margin	Uncertainty	CR
Lower	12.61	9.77	1.29
Upper	13.67	9.14	1.50

Similarly, the QMU analysis is performed on system 2. Here, the design is represented by mixed uncertainty while the only performance limit is represented by an epistemic interval. A summary of the margin and performance gate uncertainty values is shown in Table 12 as well as the resulting confidence ratio of the system.

**Table 12: Maximum Heat Load QMU Analysis Metrics from System 2**

Performance Gate	Margin	Uncertainty	CR
Upper	775.92	150.98	5.14

There are two resulting confidence ratios from the QMU analysis, one from each system. A system wide confidence level would then be the minimum of these three ratios shown to be 1.29. This value indicates the weakest system in the design; however, in this case, the margins are greater than the uncertainty and the system design may be acceptable. If not, this would indicate that a re-analysis/design of the system, the performance limits, or both may be necessary to improve the reliability of the system.

## VII. High Speed Civil Transport QMU Model Problem

The last test problem is a model for the design and analysis of a high speed civil transport (HSCT), which is used to demonstrate the QMU for an aircraft analysis and design tool subject to specific design criteria. The objective is to use stochastic expansions to represent the model, which is subject to mixed epistemic and aleatory uncertainty, and quantify the margins and uncertainties in specific design (performance) metrics.

### A. Description of the Deterministic Model

#### 1. Design

The model and analysis tool used for this model problem is the Integrated Multidisciplinary Optimization Objects (IMOO) tool developed by M4 Engineering. The IMOO system<sup>36</sup> is a multidisciplinary analysis and optimization toolset designed to address many issues for next generation vehicle applications. IMOO utilizes an object-oriented integration framework that allows users to efficiently link high fidelity analysis modules. This framework is designed to significantly reduce the problem setup time by simplifying the definition of interdisciplinary coupling, allowing the creation of complex data objects and eliminating laborious manual data conversion. Additionally, these objects reduce the need for file parsers by defining standard object interfaces. The IMOO system succeeds in sharing complex data by utilizing an object-oriented approach in which upstream modules create objects that are used by downstream modules on demand. Both the data and the methods reside in the object and downstream modules may request the data when needed. An example of this is mesh generation. IMOO implements automatic mesh generation and morphing through advanced parametric geometry and grid technology for multidisciplinary modeling.<sup>37</sup> M4 Engineering has developed a parametric grid morphing tool, Geometry Manipulation by Automatic Parameterization (GMAP<sup>38</sup>), and a parametric FEA model generator for internal structures (RapidFEM<sup>39</sup>). These tools are integrated into the framework environment so that engineers can quickly integrate FEA/CFD analyses, morph geometry, re-mesh, apply loads, and generate useful results. Through careful automation of the analysis process, the IMOO system allows configurations to be rapidly assessed, allowing many variations to be considered in a relatively short time. This facilitates the implementation of numerical optimization techniques that can be used to help determine the optimal design.

For the current effort, the configuration selected for analysis is the High Speed Civil Transport (HSCT). An illustration of a generic configuration is shown in Figure 13. Design variables used in the IMOO system model of the HSCT include the wing area, aspect ratio, sweep angle, taper ratio, spanwise location of break chord, leading edge position of break, break chord, and tip chord ratio (Figure 14).

For the QMU demonstration, a modified version of the supersonic vehicle design process was selected, as shown in Figure 15. There are five modules considered in the current study: (1) Geometry, (2) Aerodynamics, (3) Propulsion, (4) Structures, and (5) Range Performance (Breguet Range). This standard design structure

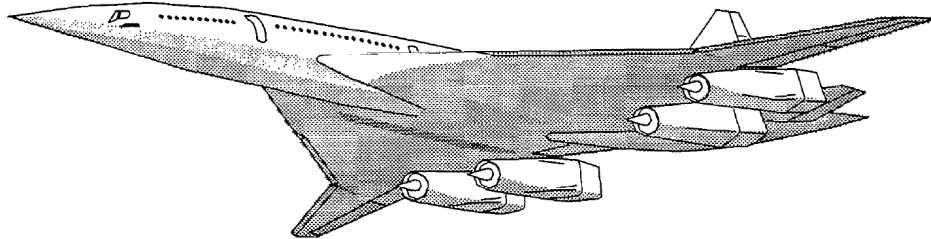


Figure 13: Generic HSCT Configuration

- **High Speed Civil Transport (HSCT)**
- **Geometric Design Variables**

- S (wing projected area)
- AR (aspect ratio)
- Sweep
- Taper
- Omega
- Eta
- Theta

Non-dimensional representation of wing break

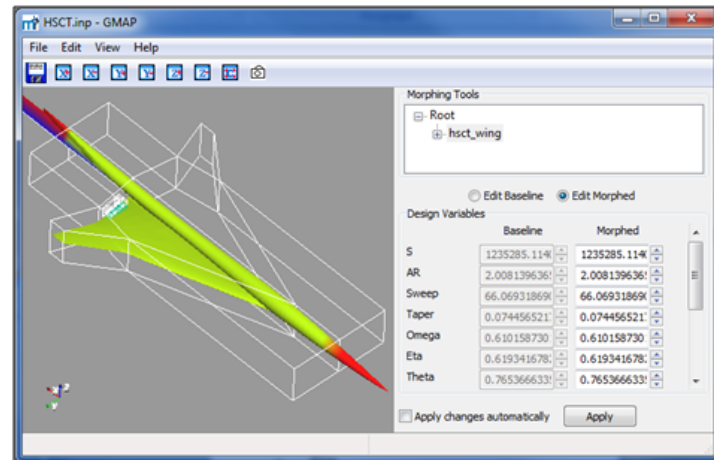


Figure 14: HSCT with Geometric Design Variables

matrix format shows the analysis modules as blue boxes on the diagonal of the matrix, and the data items used by or generated by the modules are shown as yellow boxes. The far left column of yellow boxes represents inputs to the entire process, and the far right column represents outputs from the process. More simply put, the outputs of a module are shown on the same row as the module, and the inputs are shown on the same column (for example, Propulsion Performance is an output of the Propulsion Module and an input to the Breguet Range Module). In general, module execution is shuffled to get as much information as possible into the upper-right triangle of the matrix, which represents a feed-forward path, where the module generating the data is executed prior to the module using the data. Feedback paths are possible, but require special consideration (e.g., iteration to convergence) and hence, will not be included in this demonstration.

In this process, the geometry module takes the geometric parameters and generates (through GMAP) an updated CFD model (via mesh morphing), a FEM mesh (through parametric geometry & meshing), and information for the propulsion module. Figure 16 shows the initial geometry used to develop the baseline aerodynamic and structural meshes.

The aerodynamics module calculates the vehicle aerodynamic coefficients and distributed pressures at various flight conditions for use in performance simulation and loads calculation. In order to expedite aerodynamic analyses, the current implementation of the aerodynamics module utilizes Panair<sup>40</sup> to compute aerodynamic loads. Panair (Panel Aerodynamics) solves the linearized potential flow problem for subsonic and supersonic regimes using a higher-order panel method.<sup>41-43</sup> Figure 17 shows the half model used for aerodynamic analysis.

The propulsion module utilizes the Numerical Propulsion System Simulation (NPSS)<sup>44</sup> to calculate the propulsion performance (specific fuel consumption, SFC, etc.) for use in the Breguet Range module. NPSS is a comprehensive propulsion simulation tool capable of accurately predicting aerothermodynamic behavior of jet engines in various flight regimes.

The structural module, using a NASTRAN optimization, calculates loads and structural sizing to estimate the takeoff gross weight (TOGW). The design load case simulated corresponds to a 1.5-g pull up (consistent with FAR part 25 criteria). The Breguet Range Module computes the range performance for the supersonic

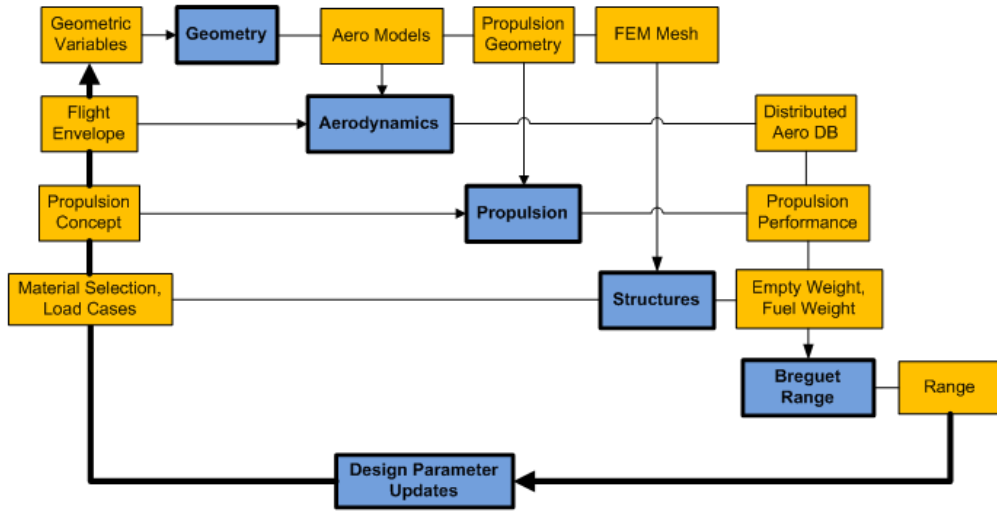


Figure 15: Supersonic Vehicle Design Structure Matrix

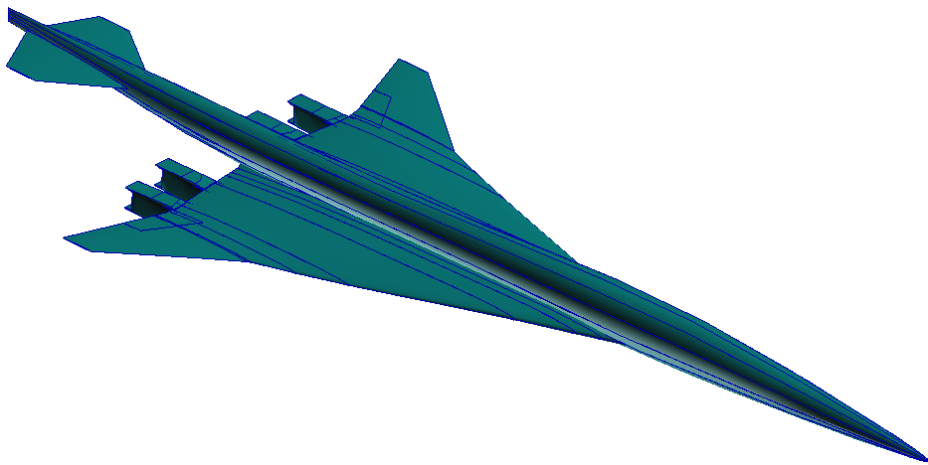


Figure 16: HSCT base geometry (shown without vertical tail)

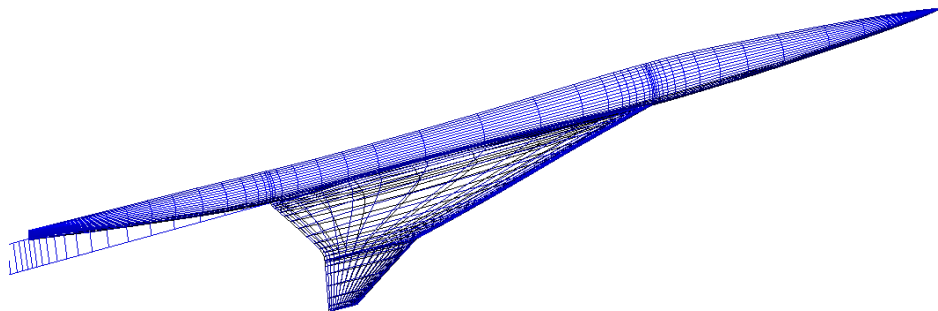


Figure 17: HSCT Panair Model (Wing-Body Wake)

vehicle based upon the outputs from the upstream modules.

For the QMU analysis of an HSCT design, two output parameters were chosen as the design quantities of interest: (1) drag coefficient and (2) range. The drag coefficient is a key parameter in aerodynamic design. This parameter directly effects key aspects of aircraft design such power plant sizing, fuel economy, and payload capability. Additionally, range is an important performance metric of an aircraft and is a

fundamental design criteria for aircraft capability. These two parameters are both outputs from the IMOO system, as discussed above. As with the previous model problems, the objective will be to perform a QMU analysis of the performance metrics when the input parameters to the analysis tool are subject to uncertainty.

## 2. Performance Limits

In this model problem, performance limits with no uncertainty were assigned to each of the design quantities of interest. This selection was made to demonstrate the QMU analysis of design problems where specific criteria or performance requirements need to be met to satisfy specific design purposes. For example, in this model problem, a minimum value to the range was prescribed as the performance limit as this is a common aircraft design quantity. Similarly, a maximum value on the drag coefficient was assigned as this parameter directly effects vehicle performance and a maximum may be used as a criteria to limit engine selection size and reduce fuel economy.

## B. Description of the Stochastic Model

### 1. Design

For the current HSCT analysis problem, four uncertain input variables were identified as possible sources of uncertainty. These parameters and their classification are shown in Table 13. Note these uncertain parameters come from both epistemic and aleatory uncertainty sources, indicating the need for a mixed uncertainty analysis.

**Table 13: HSCT Model Uncertain Parameters**

Variable	Distribution	Mean/	Std./
		Min	Max
Mach Number	Gaussian	2.0	0.02
Angle of Attack	Epistemic	2.4	2.6
Wing Sweep Angle	Gaussian	63.0	1.0
Wing Taper Ratio	Uniform	0.06	0.1

### 2. Performance Limit

The lower performance limit on the range performance was represented by single value of 2500 nmi with no uncertainty. No upper limit was assigned to the range capability of the aircraft. The drag coefficient, however, was constrained only by an upper limit of 0.009 also with no uncertainty.

## C. Uncertainty Quantification

### 1. Design

Performing the UQ in the system design condition and the performance limits is next step in the analysis. Using Eq. (2), 30 evaluations of the deterministic model were required for four uncertain variables with an OSR=2 using second order polynomial chaos expansions. The upper and lower CDFs of the output P-Boxes are given in Figures 18 and 19 for the vehicle range and drag coefficient, respectively. Note that these were obtained using the sampling approach for mixed uncertainty outlined in section III.C.

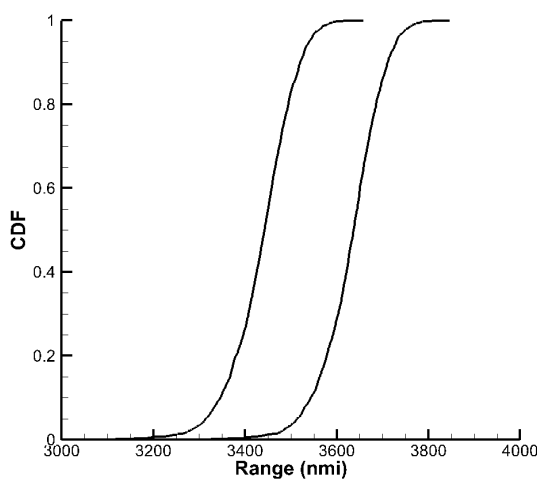


**Figure 18: System 1 Range P-Box Plot**

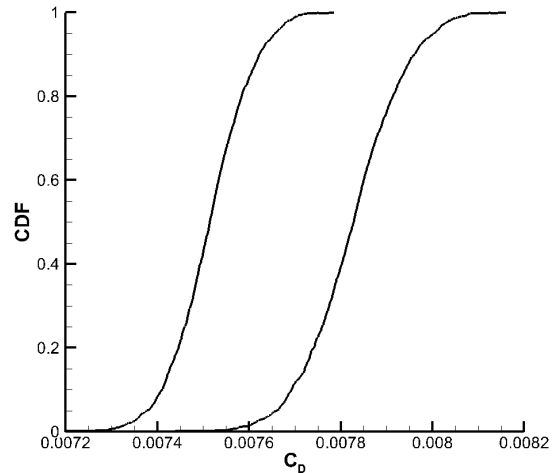


**Figure 19: System 2 Drag Coefficient P-Box Plot**

Similar to the previous model problem, it was possible to check the accuracy of the surrogate model by comparing results obtained from the actual model to those obtained from the surrogate model at the same sample location in the design space. In this study, 10 sample points, distributed evenly in the design space, were used to measure the accuracy of the surrogate models. Of the two surrogates created in this model problem, the highest mean error in the sample points was about 0.04% validating the selection of second order polynomial chaos expansions. Note that these sample points differ from the sample points used to train the surrogate model.

## 2. Performance Limits

No uncertainty quantification was performed on the performance limits for this model as both models were assigned boundaries with no uncertainty.

## D. Quantification of Margins and Uncertainties

After obtaining the uncertainty in the components of the system, it is now possible to perform the QMU analysis. A 95% confidence analysis (i.e.,  $\beta = 0.95$ ) has been selected for this problem. Using the equations and tables given in section IV. B., the margin calculations can be performed. For the range performance, the design metric was represented by mixed uncertainty. The lower performance limit of the range was a single value with no uncertainty. The drag coefficient output was also represented by mixed uncertainty and the upper performance limit was a single point value with no uncertainty. A summary of the margin and performance gate uncertainty values as well as the resulting confidence ratios of the system are given in Tables 14 and 15.

**Table 14: HSCT Model Range QMU Analysis Metrics**

Performance Gate	Margin	Uncertainty	CR
Lower	784.66	352.28	2.23

**Table 15: HSCT Model Drag Coefficient QMU Analysis Metrics**

Performance Gate	Margin	Uncertainty	CR
Upper	9.7e-4	5.15e-4	1.89

There are two resulting confidence ratios from the QMU analysis, one from each of the performance metrics. A system wide confidence level would then be the minimum of these two ratios which is shown to be 1.89. This value indicates the weakest system in the design; however, the margins are greater than the uncertainty and the system design may be acceptable.

## VIII. Conclusions

This study had two primary objectives for further advancement of the quantification of margins and uncertainties (QMU) methodologies implemented for complex aerospace systems. The first objective was to demonstrate the use of stochastic expansions, based on nonintrusive polynomial chaos, to efficiently quantify the uncertainty in system design performance metrics as well as performance boundaries. The second objective was to define procedures to measure margin and uncertainty metrics for QMU analysis of systems containing multiple types of uncertainty representation. In order to demonstrate the QMU methodologies developed in this work, three model problems were selected. These models contained design metrics and the performance limits, which included mixed (aleatory and epistemic) uncertainties.

The first model consisted of a complex system of highly nonlinear, analytical functions typically used as test functions in numerical optimization studies. The objective with this model was to demonstrate both the uncertainty quantification using stochastic expansions and the QMU approaches on a general, mathematical problem containing two, coupled non-linear systems that share common input variables. Additionally, both performance metrics and system boundaries have different uncertainty characteristics.

The second model was a multisystem, multiphysics model of a spacecraft reentry. The design consisted of two physics based systems possessing both epistemic and aleatory uncertainty. The first was a model for the reentry dynamics of a six-degree of freedom, lifting body. The performance metrics of this system were the maximum g-load experienced along the trajectory and the bank angle correction required to reach a target landing location. These are critical values in the design of a reentry system as it affects structural design of the spacecraft, the safety of any crew on board, and the design of the control system used during reentry. Performance boundaries were selected to reflect possible limitations of both performance metrics. The second system, which was coupled to the first, was a model for the stagnation point convective heat flux. Calculations were performed at multiple points along the trajectory in order to determine the maximum convective heat load experienced during reentry. The performance boundary of this metric was defined by current thermal protection material limitations and flight certifications.

The last model problem was a design and analysis tool for a high speed civil transport. The design was a baseline configuration subject to flight and geometric uncertainties. Performance metrics included range performance and drag coefficient which may be critical criteria in aircraft design. Performance limits of the two metrics were selected to reflect specific design specifications.

Overall, the work done in this study has demonstrated a computationally efficient and accurate framework for the quantification of margins and uncertainties in complex aerospace systems. Procedures were outlined to treat various types of uncertainty representation in both performance metrics and performance limits. Multiple model problems, ranging in complexity, were utilized to not only demonstrate the methodologies presented in this work, but also to iterate the importance of accurate system reliability analysis.

## Acknowledgments

Funding for this research was provided by NASA Jet Propulsion Laboratory under a STTR Phase II project grant no. NNX11CC60C (Lee D. Peterson, program manager).

## References

- <sup>1</sup>Sharp, D. H. and Wood-Schultz, M. M., "QMU and Nuclear Weapons Certification. Whats Under the Hood," *Los Alamos Science*, , No. 28, 2003, pp. 47–53.
- <sup>2</sup>Eardley, D., "Quantification of Margins and Uncertainties (QMU)," Tech. Rep. JSR-04-330 (JASON), EECS Department, University of California, Berkeley, mar 2005.
- <sup>3</sup>Pilch, M., Trucano, T. G., and Helton, J. C., "Ideas Underlying Quantification of Margins and Uncertainties (QMU): A White Paper," *Sandia National Laboratories Report*, Vol. SAND2006-5001, Sept. 2006.
- <sup>4</sup>Helton, J. C., "Conceptual and Computational Basis for the Quantification of Margins and Uncertainty," *Sandia National Laboratories Report*, Vol. SAND2009-3055, June 2009.
- <sup>5</sup>Romero, V. J., "Some Issues and Needs in Quantification of Margins and Uncertainty in Complex Coupled Systems, AIAA 2006-1989," 47<sup>th</sup> AIAA/ASME/ASCE/AHS/ASC Structures, Structural Dynamics, and Materials Conference, Newport, RI, May 2006.
- <sup>6</sup>Pepin, J. E., Rutherford, A. C., and Hemez, F. M., "Defining a Practical QMU Metric, AIAA 2008-1717," 49<sup>th</sup> AIAA/ASME/ASCE/AHS/ASC Structures, Structural Dynamics, and Materials Conference, Schaumburg, IL, April 2008.
- <sup>7</sup>Iaccarino, G., Pecnik, R., Glimm, J., and Sharp, D., "A QMU Approach for Characterizing the Operability Limits of Air-Breathing Hypersonic Vehicles," *LANL Report*, Vol. LA-UR 09-01863, 2009.

<sup>8</sup>Lucas, L. J., Owhadi, H., and Ortiz, M., "Rigorous Verification, Validation, Uncertainty Quantification and Certification Through Concentration-of-Measure Inequalities," *Computer Methods in Applied Mechanics and Engineering*, Vol. 197, 2008, pp. 4591–4609.

<sup>9</sup>Swiler, L. P., Paez, T. L., Mayes, R. L., and Eldred, M. S., "Epistemic Uncertainty in the Calculation of Margins, AIAA 2009-2249," 50<sup>th</sup> AIAA/ASME/ASCE/AHS/ASC Structures, Structural Dynamics, and Materials Conference, Palm Springs, CA, May 2009.

<sup>10</sup>Hosder, S. and Bettis, B., "Uncertainty and Sensitivity Analysis for Reentry Flows with Inherent and Model-Form Uncertainties," *Journal of Spacecraft and Rockets*, Vol. 49, No. 2, 2012, pp. 193–206.

<sup>11</sup>Bettis, B., Hosder, S., and Winter, T., "Efficient Uncertainty Quantification in Multidisciplinary Analysis of a Reusable Launch Vehicle, AIAA 2011-2393," 17<sup>th</sup> AIAA International Space Planes and Hypersonic Systems and Technologies Conference, San Francisco, CA, April 2011.

<sup>12</sup>Hosder, S., Walters, R. W., and Balch, M., "Efficient Sampling for Non-Intrusive Polynomial Chaos Applications with Multiple Uncertain Input Variables, AIAA 2007-1939," 48<sup>th</sup> AIAA/ASME/ASCE/AHS/ASC Structures, Structural Dynamics, and Materials Conference, Honolulu, HI, April 2007.

<sup>13</sup>Hosder, S., Walters, R. W., and Balch, M., "Point-Collocation Nonintrusive Polynomial Chaos Method for Stochastic Computational Fluid Dynamics," *AIAA Journal*, Vol. 48, No. 12, 2010, pp. 2721–2730.

<sup>14</sup>Eldred, M. S., "Recent Advances in Non-Intrusive Polynomial Chaos and Stochastic Collocation Methods for Uncertainty Analysis and Design, AIAA 2009-2274," 50<sup>th</sup> AIAA/ASME/ASCE/AHS/ASC Structures, Palm Springs, CA, May 2009.

<sup>15</sup>Witteveen, J. A. S. and Bijl, H., "Efficient Quantification of the Effect of Uncertainties in AdvectionDiffusion Problems Using Polynomial Chaos," *Numerical Heat Transfer*, Vol. 53, No. 5, 2008, pp. 437–465.

<sup>16</sup>Han, D. and Hosder, S., "Inherent and Model-Form Uncertainty Analysis for CFD Simulation of Synthetic Jet Actuators, AIAA 2012-0082," 48<sup>th</sup> AIAA Aerospace Sciences Meeting, Nashville, TN, Jan. 2012.

<sup>17</sup>Walters, R. W. and Huyse, L., "Uncertainty Analysis for Fluid Mechanics with Applications," Tech. rep., ICASE 2002-1, NASA/CR-2002-211449, NASA Langley Research Center, Hampton, VA, 2002.

<sup>18</sup>West IV, T. K., Hosder, S., and Johnston, C. O., "A Multi-Step Uncertainty Quantification Approach Applied to Hypersonic Reentry Flows, AIAA 2011-2524," 51<sup>st</sup> AIAA Aerospace Sciences Meeting, Grapevine, TX, Jan. 2013.

<sup>19</sup>Lockwood, B. and Mavriplis, D., "Gradient-Based Methods for Uncertainty Quantification in Hypersonic Flows," *Computers and Fluids Journal*, Vol. 85, Oct. 2013, pp. 27–38.

<sup>20</sup>Roderick, O., Anitescu, M., and Fischer, P., "Polynomial Regression Approaches Using Derivative Information for Uncertainty Quantification," *Nuclear Science and Engineering*, Vol. 164, No. 2, 2010, pp. 122–139.

<sup>21</sup>Oberkampf, W. L., Helton, J. C., and Sentz, K., "Mathematical Representation of Uncertainty, AIAA 2001-1645," 3<sup>rd</sup> Non-Deterministic Approaches Forum, Seattle, WA, April 2001.

<sup>22</sup>Eldred, M. and Swiler, L., "Efficient Algorithms for Mixed Aleatory-Epistemic Uncertainty Quantification with Application to Radiation-Hardened Electronics," *Sandia National Laboratories Report*, Vol. SAND2009-5805, Sept. 2009.

<sup>23</sup>De Zaiacomo, G., M., K., Haya, R., and Penin, L. F., "Robust Skip Entry Guidance and Control for a Capsule Returning from Lunar Orbit, AIAA 2009-5771," *AIAA Guidance, Navigation, and Control Conference*, Chicago, IL, Aug. 2009.

<sup>24</sup>Hoelscher, B., "Orion Entry, Descent, and Landing, AIAA 2007-6428," *AIAA Guidance, Navigation, & Control Conference*, Hilton Head, SC, Aug. 2007.

<sup>25</sup>Berger, K., "Aerothermodynamic Testing of the Crew Exploration Vehicle in the LaRC 20-Inch Mach 6 and 31-Inch Mach 10 Tunnels, AIAA 2008-1225," 46<sup>th</sup> AIAA Aerospace Sciences Meeting, Reno, NV, Jan. 2008.

<sup>26</sup>Xue, S. and Lu, P., "Constrained Predictor-Corrector Entry Guidance," *Journal of Guidance, Control, and Dynamics*, Vol. 33, No. 4, 2010, pp. 1273–1281.

<sup>27</sup>Brunner, C., , and Lu, P., "Skip Entry Trajectory Planning and Guidance, AIAA 2007-6777," *AIAA Guidance, Navigation, and Control Conference*, Hilton Head, SC, Aug. 2007.

<sup>28</sup>D'Souza, S. and Sarigul-Klijn, N., "Investigation of Trajectory Generation for a Mission Adaptive Planetary Entry Guidance Algorithm, AIAA 2012-4508," *AIAA Atmospheric Flight Mechanics Conference*, Minneapolis, MN, Aug. 2012.

<sup>29</sup>Hoelscher, B. R., Strahan, A. L., Stachowiak, S. J., and Loe, G. R., "Orion Entry Flight Control Modifications and Performance, AIAA 2008-7152," *AIAA Guidance, Navigation, and Control Conference*, Honolulu, HI, Aug. 2008.

<sup>30</sup>Fay, J. A. and Riddell, F. R., "Theory of stagnation point heat transfer in dissociated air," *Journal of Aeronautical Sciences*, Vol. 25, No. 25, 1958, pp. 73–85.

<sup>31</sup>Anderson Jr., J. D., *Hypersonic and High-Temperature Gas Dynamics*, American Institute of Aeronautics and Astronautics, Reston, VA, 2nd ed., 2006.

<sup>32</sup>Tannehill, J. C. and Mugge, P. H., "Improved Curve Fits for the Thermodynamic Properties of Equilibrium Air Suitable for Numerical Computation Using Time-Dependent or Shock-Capturing Methods," Tech. rep., NASA/CR-2470, Oct. 1974.

<sup>33</sup>Trumble, K., Cozmuta, I., Sepka, S., Jenniskens, P., and Winter, M., "Postflight Aerothermal Analysis of Stardust Sample Return Capsule," *Journal of Spacecraft and Rockets*, Vol. 47, No. 5, 2010, pp. 765–774.

<sup>34</sup>Chen, Y., Squire, T., Laub, B., and Wright, M., "Monte Carlo Analysis for Thermal Protection System Design, AIAA-Paper 2006-2951," 9<sup>th</sup> AIAA/ASME Joint Thermophysics and Heat Transfer Conference, San Francisco, CA, June 2006.

<sup>35</sup>Shang, J. and Surzhikov, T., "Simulating Stardust Earth Reentry with Radiation Heat Transfer," *Journal of Spacecraft and Rockets*, Vol. 48, No. 3, 2011, pp. 385–396.

<sup>36</sup>Doyle, S., Alston, K., and Winter, T., "Developing the Aerodynamics Module for the Integrated Multidisciplinary Optimization Object System, AIAA 2011-8," 49<sup>th</sup> AIAA Aerospace Sciences Meeting, Orlando, FL, Jan. 2011.

<sup>37</sup>Raymondson, C. T., Baker, M. L., Doyle, S. P., and Young, S. M., "Geometry Manipulation by Automatic Parameterization (GMAP), AIAA 2008-6027," 12<sup>th</sup> AIAA/ISSMO MDAO Conference, Victoria, British Columbia Canada, Sept. 2008.

<sup>38</sup>Dahlin, A. and Baker, M. L., "GMAP Mesh User's Manual," Tech. rep., M4 Engineering, 2010.

<sup>39</sup>Stuewe, D. and Baker, M. L., "RapidFEM User's Manual," Tech. rep., M4 Engineering, 2010.

<sup>40</sup>Saarlis, G. R., Tinoco, E. N., Lee, J. L., and Rubbert, P. E., "User's Guide PAN AIR Technology Program for Solving Potential Flow about Arbitrary Configurations," Tech. rep., 1992.

<sup>41</sup>Johnson, F. T. and Rubbert, P. E., "Advanced Panel-Type Influence Coefficient Methods Applied to Subsonic Flows, AIAA 75-50," July 1975.

<sup>42</sup>Ehlers, F. E., Johnson, F. T., and Rubbert, P. E., "A Higher Order Panel Method for Linearized Supersonic Flow, AIAA 76-381," July 1976.

<sup>43</sup>Ehlers, F., "A Higher Order Panel Method for Linearized Supersonic Flow," Tech. rep., NASA/CR 3062, 1979.

<sup>44</sup>Claus, R., Evans, A., Lylte, J., and Nichols, L., "Numerical Propulsion System Simulation," *Computing Systems in Engineering*, Vol. 2, 1991, pp. 357-364.